ACS Catalysis

Research Article

pubs.acs.org/acscatalysis

Hydrothermal Synthesis of Graphene-TiO_2 Nanotube Composites with Enhanced Photocatalytic Activity

Sanjaya D. Perera,[†] Ruperto G. Mariano,[†] Khiem Vu,[†] Nijem Nour,[‡] Oliver Seitz,[‡] Yves Chabal,[‡] and Kenneth J. Balkus, Jr.*[,†]

[†]Department of Chemistry and the Alan G. MacDiarmid Nanotech Institute, 800 West Campbell Rd, University of Texas at Dallas, Richardson, Texas 75080, United States

[‡]Laboratory for Surface and Nanostructure Modification, Department of Material Science and Engineering, 800 West Campbell Rd, University of Texas Dallas, Richardson, Texas 75080, United States

Supporting Information

ABSTRACT: In this study, TiO_2 nanotube (TNT)/reduced graphene oxide (hGO) composites were prepared by an alkaline hydrothermal process. This was achieved by decorating graphene oxide (GO) layers with commercially available TiO_2 nanoparticles (P90) followed by hydrothermal synthesis, which converts the TiO_2 nanoparticles to small diameter (~9 nm) TNTs on the hGO surface. The alkaline medium used to synthesize the TNTs simultaneously converts GO to deoxygenated graphene oxide (hGO). Compared to GO, the hGO has a ~70% reduction of oxygenated species after alkaline hydrothermal treatment. The graphene nature of hGO in the composites was confirmed by X-ray diffraction (XRD), Raman, FTIR, and X-ray photoelectron spectroscopy (XPS) analysis. The photocatalytic performance of the hGO-TNT composites was evaluated for the photodegradation of malachite green. It was found that the ratio of hGO to TNT in the composites significantly affects the photocatalytic activity. Higher amounts of hGO in hGO-TNT composites showed lower photocatalytic activity than pure TNTs. The composite with 10% hGO showed the highest photocatalytic activity, with a 3-fold enhancement in photocatalytic efficiency over pure TNTs. It is expected that the synthesis of "high surface area-small diameter" TiO_2 nanotubes and simultaneous conversion of GO to graphene like hGO "without using strong reducing agents" could be a promising strategy for preparing other types of carbon based TiO_2 nanotube composite photocatalysts.

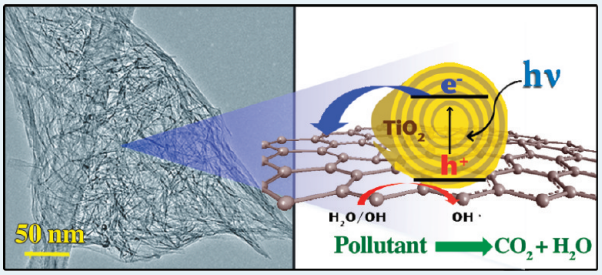

KEYWORDS: *TiO_2 nanotube photocatalyst, graphene-TiO_2 nanotube composites, graphene-TiO_2 nanotube photocatalyst*

INTRODUCTION

Titanium dioxide (TiO_2) is one of the most widely investigated semiconducting metal oxides that exhibits photocatalytic activity and is used in a wide range of applications.[1−5] When TiO_2 is irradiated with UV light, electrons are excited from the valence band (VB) to the conduction band (CB), creating electron−hole pairs, which are mainly responsible for the photocatalytic activity. However, the photogenerated electron−hole pairs have faster recombination rates than the rate of chemical interaction between TiO_2 and adsorbed pollutants, reducing the photocatalytic efficiency. Therefore, the challenge is to prevent electron−hole pair recombination and improve the photocatalytic activity of TiO_2.

A series of strategies have been developed to synthesize TiO_2 based nanocomposites for the inhibition of high intrinsic electron−hole pair recombination as well as further modification of the band gap of the composite.[6−9] For example, doping,[10] combining with metal oxides,[11] quantum dots,[6] semiconductors,[12] and carbon materials. In particular, there is growing interest in the combination of carbon based materials and TiO_2 to enhance photocatalytic performance. It has been reported that, TiO_2-carbon nanotube composites show enhanced photocatalytic activity because of electron transfer from TiO_2 to carbon nanotubes (CNTs) which promotes charge separation and stabilization.[13,14] Unfortunately, the high production cost of CNTs, the presence of mixed metallic and semiconducting CNTs, impurities in CNTs, and the non-dispersive nature of CNTs in common solvents greatly limits the potential application of CNTs on a large scale. In contrast, other allotropes of carbon such as graphene are gaining attention because of lower cost and ease of processing graphene based composite materials.

Graphene, a single layer two-dimensional graphite structure, exhibits exceptional electrical, mechanical, and thermal properties such as high electron mobility (250,000 $cm^2/(V\ s)$), Young's modulus (1 TPa), and thermal conductivity (5000 $W\ m^{-1}\ K^{-1}$).[15,16] Because of the economical cost and superior properties, graphene has attracted significant attention for

Received: November 29, 2011
Revised: April 15, 2012
Published: April 18, 2012

various applications such as, nanoelectronics,[17] energy storage devices,[18] photovoltaics and catalysis.[19,20] Different approaches have been developed to prepare individual graphene sheets or a few layers of graphene by exfoliating naturally occurring graphite flakes.[21−24] The chemical exfoliation of graphite to individual graphene oxide (GO) layers using strong oxidizing agents has become the most common and well-known technique, which introduces oxygen functional groups.[25] The presence of these functional groups makes the GO sheets readily soluble in many solvent systems and facilitates further surface modification.[26,27] However, exfoliated GO exhibits poor electronic conductivity because of the interruption of the π system by substitution with oxygen functional groups. Therefore, various reducing agents such as N_2H_4,[28] $NaBH_4$,[29] and alcohols[30] have been used to reduce GO to restore the sp^2 hybridized network and increase the electronic conductivity. The ability of reduced graphene to store and shuttle electrons have important implications in semiconductor-graphene and metal nanoparticle-graphene composites. In particular, reduced graphene sheets provide two-dimensional mats for nanostructured catalyst assemblies.

There have been several reports highlighting the improvements in photocatalytic activity of TiO_2 nanoparticle-reduced graphene composites for the degradation of organic molecules and photocatalytic splitting of water.[2,31−35] Zhang and coworkers prepared a TiO_2 nanoparticle-graphene composite and reported enhanced photocatalytic activity for the degradation of methylene blue,[36] Xiaoyan et al. demonstrated the feasibility of water splitting to produce H_2 by using TiO_2 nanoparticles on graphene and observed higher photocatalytic activity than that of TiO_2 nanoparticles alone.[37] Despite these promising results, the TiO_2 nanoparticles tend to agglomerate and have poor interfacial contact with the graphene surface because of the nanoparticle's nearly spherical shape. Therefore, a form of TiO_2 that provides maximum interfacial contact with graphene surface without aggregating is an essential factor for improving the photocatalytic performance of graphene-TiO_2 composites. This will facilitate the charge separation and electron transfer from TiO_2 to graphene upon irradiation. In contrast to TiO_2 nanoparticles, TiO_2 nanotubes (TNTs) have much higher surface area (inner and outer surface) with an enormous number of active sites. Moreover, a greater degree of interfacial contact associated with the interface between TNTs and graphene should favor charge separation, and the high aspect ratio of TNTs enhances the photocatalytic activity.[13] Although, there have been numerous attempts to prepare different photocatalysts with reduced graphene-TiO_2, there are currently no reports on growing TiO_2 nanotubes on reduced graphene sheets. Thus, the combination of high surface area TiO_2 nanotubes and reduced graphene may improve charge separation and stabilization, which could enhance the photocatalytic activity.

Herein, we report a facile route for the growth of TiO_2 nanotubes on reduced graphene oxide sheets via hydrothermal synthesis under basic conditions. Interestingly, while TNTs were grown on the GO surface, a simultaneous deoxygenation of GO to reduced graphene oxide (hGO) was observed. The graphene content of hGO present in the hGO-TNT composites is comparable to chemically reduced graphene oxides.[29,38] The reduced graphene/TiO_2 nanotube (hGO-TNT) composites exhibit excellent photocatalytic activity toward the degradation of malachite green. The enhancement of the photocatalytic activity of hGO-TNT could be ascribed to the favorable charge transfer kinetics of graphene structure and higher photocatalytic activity of TNTs.

EXPERIMENTAL SECTION

Materials. TiO_2 nanoparticles (P90) were obtained from Evonik-Degussa. Graphite powder was purchased from Sigma Aldrich. H_2SO_4 (EMD chemicals), HCl (Fischer Scientific), $NaNO_3$ (Sigma Aldrich), NaOH (Alfa Aesar), and $KMnO_4$ (Baker analyzed) were used as received. Malachite green oxalate was purchased from Alfa Aesar.

Characterization. X-ray powder diffraction (XRD) patterns were obtained using a Rigaku Ultima IV diffractometer (Cu K_α radiation), Raman spectra was collected using a JY Horiba HR-800 spectrophotometer. Fourier Transform Infrared spectra (FTIR) were acquired using a AVATAR 360 FT-IR spectrophotometer. Transmission electron microscope (TEM) images and Energy-dispersive X-ray spectra (EDX) were obtained using a JEOL JEM-2100 TEM at 200 kV (JEOL Co. Ltd.). Scanning electron microscope (SEM) images and EDX spectra were collected using a Leo 1530 VP field emission electron microscope. UV−vis spectra were recorded using a Shimadzo UV-1601PC spectrometer. Photoluminescence spectra (PL) were acquired at room temperature using a PerkinElmer LS55 Luminescence spectrophotometer in diffuse reflection mode and an excitation wavelength of 400 nm. X-ray photoelectron spectroscopy (XPS) measurements were performed ex situ, using a Perkin-Elmer PHI System. The photoelectrons were excited using monochromatic Al K α radiation ($h\nu$ = 1486.6 eV), and the spectra were acquired with 45° emission angle, using a 0.125 eV step size and a pass energy of 29.35 eV in the hemispherical analyzer. The nominal pressure in the analysis chamber was 3×10^{-9} Torr.

Synthesis of Graphene Oxide. GO was synthesized using a modified Hummer's method.[25] Briefly, 0.5 g of graphite and 0.5 g of $NaNO_3$ in 23 mL of 12.1 M H_2SO_4 were stirred in an ice bath for 15 min. Then 4.0 g of $KMnO_4$ was slowly added in an ice bath to yield a purple-green mixture. This suspension was transferred to a 40 °C water bath and magnetically stirred for 90 min. The dark brown colored paste was diluted with the slow addition of 50 mL of deionized water (DI) and allowed to stir for a further 10 min. A 6 mL portion of H_2O_2 was slowly added to quench the solution to produce a golden-brown sol. A further 50 mL of DI water was added, and the resultant product centrifuged and washed with warm DI water repeatedly to adjust the pH to ∼6. Finally the product was dried at 80 °C for 24 h.

Synthesis of hGO-TNT Composites. TNT composite with different GO compositions were prepared through an alkaline hydrothermal treatment. First, (w/w) ratio of 5%, 10%, 15%, and 20% of GO was sonicated in 30 mL of DI water for 1 h to achieve uniform dispersions of GO. Next, TiO_2 (P90) powder was added slowly to the GO dispersions while stirring. The TiO_2 /GO mixture was further stirred for 1 h to ensure complete mixing. Then 10.5 g of NaOH was added, and the mixture was transferred to a Teflon-lined autoclave. The mixture was then heated at 120 °C under static condition for 24 h. The resulting gray colored gel was washed with 0.1 M HCl solution and stirred overnight at room temperature. The final product was washed with DI water several times, centrifuged, dried at 80 °C, and annealed at 300 °C for 60 min.

Photocatalytic Measurements. Before photocatalytic measurements the samples were ground using a Wig-L-Bug to obtain a fine powder. The photocatalytic activity of the

dx.doi.org/10.1021/cs200621c | ACS Catal. 2012, 2, 949−956

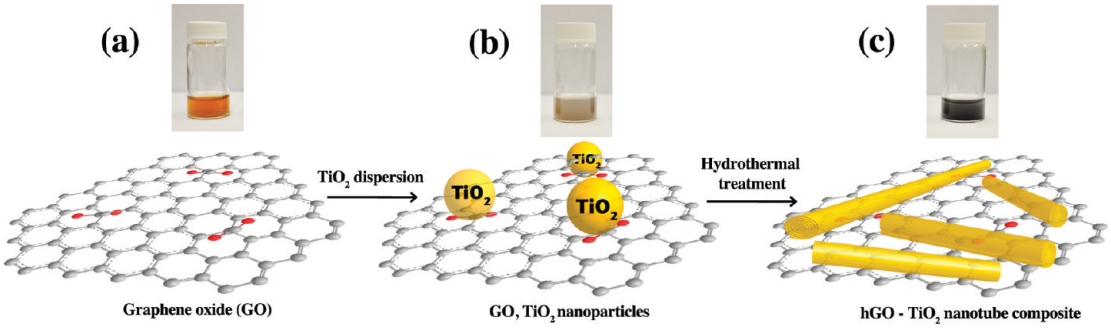

Figure 1. Graphical illustration of the synthesis of TiO_2 nanotubes on hGO sheets. The GO sheets (a) were coordinated with TiO_2 nanoparticles (b), and then converted to TNTs on hGO (c). The digital images show the color changes of the aqueous dispersions in each step.

hGO-TNT composites was evaluated for the degradation of malachite green oxalate (13.1 mg/L) in H_2O. First 20 mg of the catalyst was combined with the 100 mL of the dye solution in a 250 mL quartz round-bottom flask and placed inside a dark box equipped with a water-cooled mercury lamp (450W, quartz Hanovia). The mixture was stirred in the dark for 1 h to establish baseline correction after adsorption of the dye to the catalyst. Then it was irradiated with the light generated from the 450 W mercury lamp. Five milliliter aliquots were withdrawn at certain time intervals, centrifuged to remove the catalyst, and the highest absorbance was measured by UV−vis spectroscopy.

RESULTS AND DISCUSSION

Characterization of GO and hGO-TNT Composites. The process for the preparation of hGO-TNT composites is illustrated in Figure 1. Because of the strong hydrophilic nature of oxygen functionalities on GO sheets, they are readily soluble in aqueous medium. Oxygen groups such as carboxylates facilitate the binding of TiO_2 nanoparticles. The homogeneous colloidal suspension of exfoliated graphene oxide in water is golden brown (Figure 1a). Vigorous stirring of commercially available TiO_2 nanoparticles (P90) in GO suspensions results in anchoring of TiO_2 nanoparticles on to the GO surfaces (Figure 1b). The TiO_2 nanoparticles can be readily converted to TNTs by a hydrothermal process (Figure 1c). The color changes occur during each step is illustrated in digital photographs of the aqueous dispersions in Figure 1a, b, and c. It can be clearly seen that the color of the TiO_2/GO dispersion became dark black after the hydrothermal treatment. The dark black color of the hGO-TNT composites is consistent with partial conversion of golden brown GO to reduced graphene.[39] Recently Jonathan and co-workers observed a similar color change upon washing GO with NaOH. It was also concluded that GO consists of strongly adhered oxidative debris on the surface that can be detached to yield graphene like sheets. The hydrothermal process to prepare TNTs involves 10 M NaOH at 120 °C for 24 h.[40] These conditions may also deoxygenate the GO to an even a greater extent than just washing.[40,41]

Figure 2a shows a XRD pattern of GO with a characteristic (002) peak at 2θ = 10.5°, having an interlayer distance of ∼0.9 nm. The oxygen functional groups attached to both sides of the graphite flakes create atomic defects (sp^3 bonding) in the graphite structure and tend to exfoliate to a few layers or individual layers of GO in an aqueous medium.[42] Compared to GO, complete disappearance of the strong (002) peak in all composites suggests successful conversion of GO to reduced

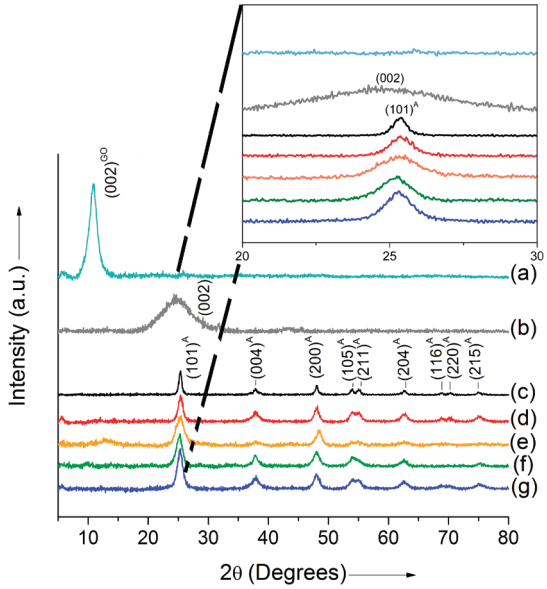

Figure 2. XRD patterns of (a) GO, (b) hGO, (c) TNTs, (d) 5%-hGO-TNT, (e) 10%-hGO-TNT, (f) 15%-hGO-TNT and (g) 20%-hGO-TNT. Inset XRD pattern showing the 20−30 degrees region.

graphene in the final composites. Since, anatase TiO_2 (101) and graphene (002) XRD peaks are located at ∼26° and 25° 2θ, it is hard to distinguish both peaks as a result of the broad reflection from the nanotubes. Pure hGO prepared in the absence of TiO_2 shows a strong (002) graphene reflection at 26.5°, which is a clear indication of the conversion of hGO to graphene.[38] The hGO-TNT composites with different hGO compositions exhibit the characteristic (101), (004), (200), (105), (211), (204), (116), (220), and (215) reflections that correspond to the anatase crystal phase (JCPDS PDF#: 00-021-1272) (Figure 2(d−g)). The (101) peak for composites is much broader than that of TNTs (Figure 2 inset). Peak broadening suggest that the lattice structure of TiO_2 is distorted by the interaction with hGO.[43] Compared to bulk TNTs, the crystalline structure of TNTs on hGO is less developed.[44] The average crystal size of the TNTs and hGO-TNT samples were calculated using the Scherrer equation based on the XRD peak broadening of the (101) peak (Supporting Information, Table S1). The average crystal sizes calculated using Scherrer equation for the composites were in the range of ∼6−8 nm, which is much smaller than TNTs (14.2 nm). This is consistent with the TEM results (vide infra) that further show the hGO affects the crystal growth of TNTs.

dx.doi.org/10.1021/cs200621c | ACS Catal. 2012, 2, 949−956

Raman spectroscopy can also provide information on the structure of the TNTs and the reduced graphene. Figure 3

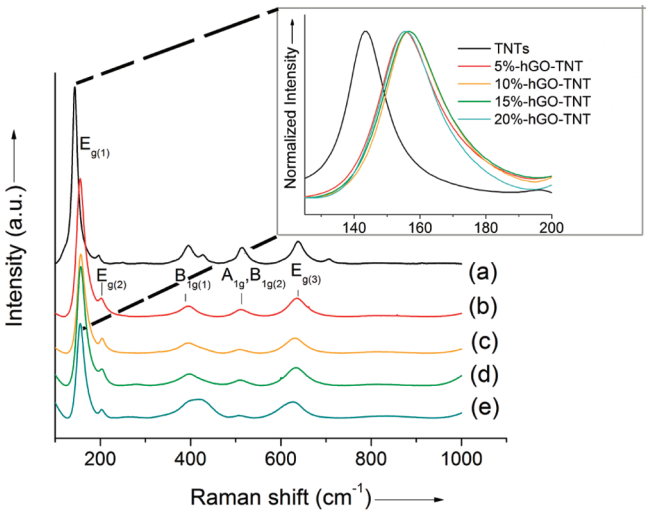

Figure 3. Raman spectra of TNTs (a), 5%-hGO-TNT (b), 10%-hGO-TNT (c), 15%-hGO-TNT (d), and 20%-hGO-TNT (e). Inset Raman spectra showing the blue shift of the E_g bands of the composites.

shows the Raman spectra of the composites prepared with different ratios of GO/TiO_2. The Raman active 144 cm^{-1}(E_g), 399 cm^{-1}(B_{1g}), 513 cm^{-1}(A_{1g}), and 638 cm^{-1}(E_g) modes for the composites match with the anatase structure of the TNTs. In addition, the peak corresponding to the E_g mode for all composites are broader and significantly blue-shifted from 143 cm^{-1} to 155 cm^{-1} (Figure 3, inset). The peak shift and broadening of the Raman spectra were analyzed using the most intense 144 cm^{-1} (E_g) peak. The peak position and broadening of the Raman spectrum is mainly affected by the size of the nanomaterial as well as defects and temperature.[45,46] It was reported that the laser induced local heating of the sample can also broaden and shift peaks. However, in this investigation we used the same laser source for recording all Raman spectra. Hence, local heating and different excitation power outputs caused by the laser can be ruled out as a source of any shifts. Therefore, the blue shift and broadening of the Raman peak for the composites are attributed to the surface pressure or phonon confinement effects that are typically observed in nanomaterials.[44] According to thoughts on confinement effects, peak broadening and shifts are observed for a change in the crystal size of poorly crystalline materials.[47,48] Both the XRD pattern and Raman spectrum of bulk TNTs show intense peaks compared to the composites. Compared to bulk TNTs, the E_g bands for the composites exhibit asymmetric broadening. The asymmetry of the Raman peak suggests that there is a contribution from phonon confinement effects to the line shape of the Raman spectra or a change in the size of nanomaterial.[44] As previously reported for carbon nanotube/TiO_2 composites reported for TiO_2 composites, the blue shift of the E_g band can be attributed to the phonon confinement effect because of the decrease in the particle size of TiO_2 and the strain developed on the TNTs/hGO surface.[48] This is a clear indication that the composite displays a strong chemical interaction between TNTs and hGO sheets, which is an essential for efficient electron transfer kinetics.

Raman spectroscopy is also widely used for the characterization of the electronic structure of carbon products. A change in Raman band intensity and shifts provide information on the nature of carbon−carbon bonds and defects. The Raman spectra in Figure 4 show the characteristic D and G bands at

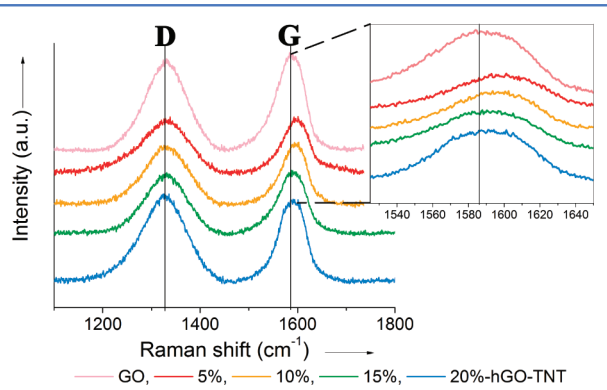

Figure 4. Characteristic D and G bands of GO and hGO-TNT composites. (inset) G band of GO and hGO-TNT composites. Compared to GO, G band of the composites is blue-shifted.

1347 cm^{-1} and 1604 cm^{-1} found in GO and the composite. The D band is a common feature for sp^3 defects in carbon, and the G band provides information on in plane vibrations of sp^2 bonded carbons.[49,50] The intensity ratio of the D band to the G band usually reflects the order of defects in GO or graphene. Compared to GO, hGO-TNT composites show two differences in the Raman spectra. First, the calculated I_D/I_G of the hGO-TNT samples were lower than that of GO, indicating a lower density of defects present in hGO. Second, the G band shifts by ~7 cm^{-1} (Figure 4, inset). The calculated I_D/I_G ratio of GO was 1.02, while 10% hGO-TNT was 0.943. The decrease in the I_D/I_G ratio is a clear indication of the increase in the number of graphene layers.[51] However, it has been previously reported that an increase in the I_D/I_G ratio during solvothermal processing or chemical reduction is also due to the fragmentation of sp^2 domains.[52,53] The decreasing of I_D/I_G ratio in the composites suggests that the hydrothermal method we used results in more graphene content without decreasing the average size of the sp^2 domain and retaining large sp^2 domains. Moreover, the lower I_D/I_G ratio indicates a better defect repair mechanism. On the basis of the I_D/I_G, the presence of lower defect levels in NaOH treated GO samples is consistent with Sun's work.[54] The blueshift of the G band can be attributed to the conversion of graphite to graphene sheets or the resonance of isolated double bonds at higher frequencies.[51] Therefore, both the change in Raman band intensity and the blue shift of the G band provide clear evidence for the presence of graphene in the composites.

The FTIR spectrum of GO (Supporting Information, Figure S1) shows strong peaks corresponding to oxygen functional groups such as, carboxylates C−O (1050 cm^{-1}), epoxide C−O−C (1230 cm^{-1}), and ketones (1700 cm^{-1}). The broad band at 1590 cm^{-1} can be assigned to in-plane vibrations of aromatic C=C sp^2 hybridized carbons in graphene. The intensity of C=O peak at 1726 cm^{-1} and sharp peaks at spectral region (800−1500 cm^{-1}) are significantly decreased in the hGO-TNT composite.[36,55,56] In contrast, the lack of oxygen features in the composites indicates the conversion of GO to hGO during hydrothermal treatment. Typically Ti−O−Ti and Ti−O−C bonds show low frequency bands around 690 cm^{-1} and 798 cm^{-1} respectively.[36] Therefore, the broad band at the low frequency region in the composite can be considered a

dx.doi.org/10.1021/cs200621c | ACS Catal. 2012, 2, 949−956

combination of Ti−O−Ti and Ti−O−C vibrations because of the chemical interaction of TNTs with the hGO. The above results confirmed the reduction of GO and the chemical coupling of TNTs and hGO.

According to the XPS survey spectrum (Supporting Information, Figure S2), the hGO-TNT composite contains Ti, O, and C with binding energies corresponding to Ti $2p_{3/2}$, Ti $2p_{1/2}$, O 1s, and C 1s. The XPS peaks at 458.6 and 464.4 eV in Supporting Information, Figure S3 are attributed to the binding energies of the Ti $2p_{3/2}$ and $2p_{1/2}$ electrons.[57] Figure 5a shows the XPS spectrum of GO with the symmetric C 1s peak at 284.4 eV for C−C bonds. Additionally, the oxygen functionalities attached to the carbons show deconvoluted peaks for C−O (285.9 eV), C═O (289.0 eV) at higher binding energies.[38,40] The deconvoluted XPS data for the C 1s electrons of the composite shows a dramatic decrease in the carbon−oxygen species in hGO (Figure 5b). The C:O ratio in GO and hGO-TNT determined using the integrated areas under the C 1s peak are ∼1:0.9 and ∼1:0.29 respectively. This suggests that the hydrothermal synthesis significantly reduces C−O bondings, thereby converting GO to graphene. The atomic ratio of C/O ratio represents the degree of reduction. On the basis of previous reports, the calculated C/O ratio for hydrazine reduced GO is 3.62 while the calculated C/O ratio for the deoxygenated GO is 3.45. Both reduction methods yield similar C/O ratios, with hydrazine reduced GO having a slightly higher C/O ratio. We interpret this experimental evidence to indicate that the alkaline hydrothermal treatment results in a greater degree of reduction compared with chemical methods.[29,38]

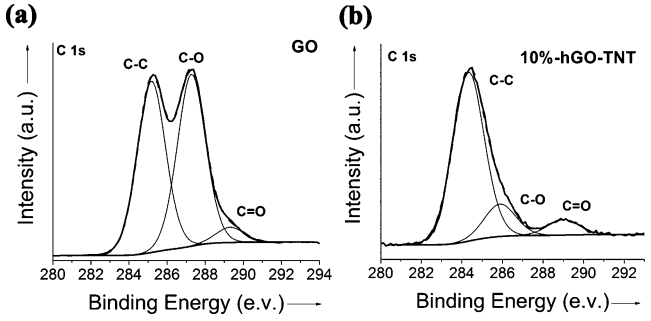

Figure 5. Deconvoluted peaks of XPS core levels of (a) C 1s of GO and (b) C 1s of 10%-hGO-TNT electrons.

Morphology of GO and hGO-TNT Composite. SEM analysis shows the TNTs are anchored on to the hGO sheets after hydrothermal treatment (Figure 6). Figure 6a shows the SEM image of GO before the attachment of TNTs. This sheet morphology is retained even after the hydrothermal treatment,

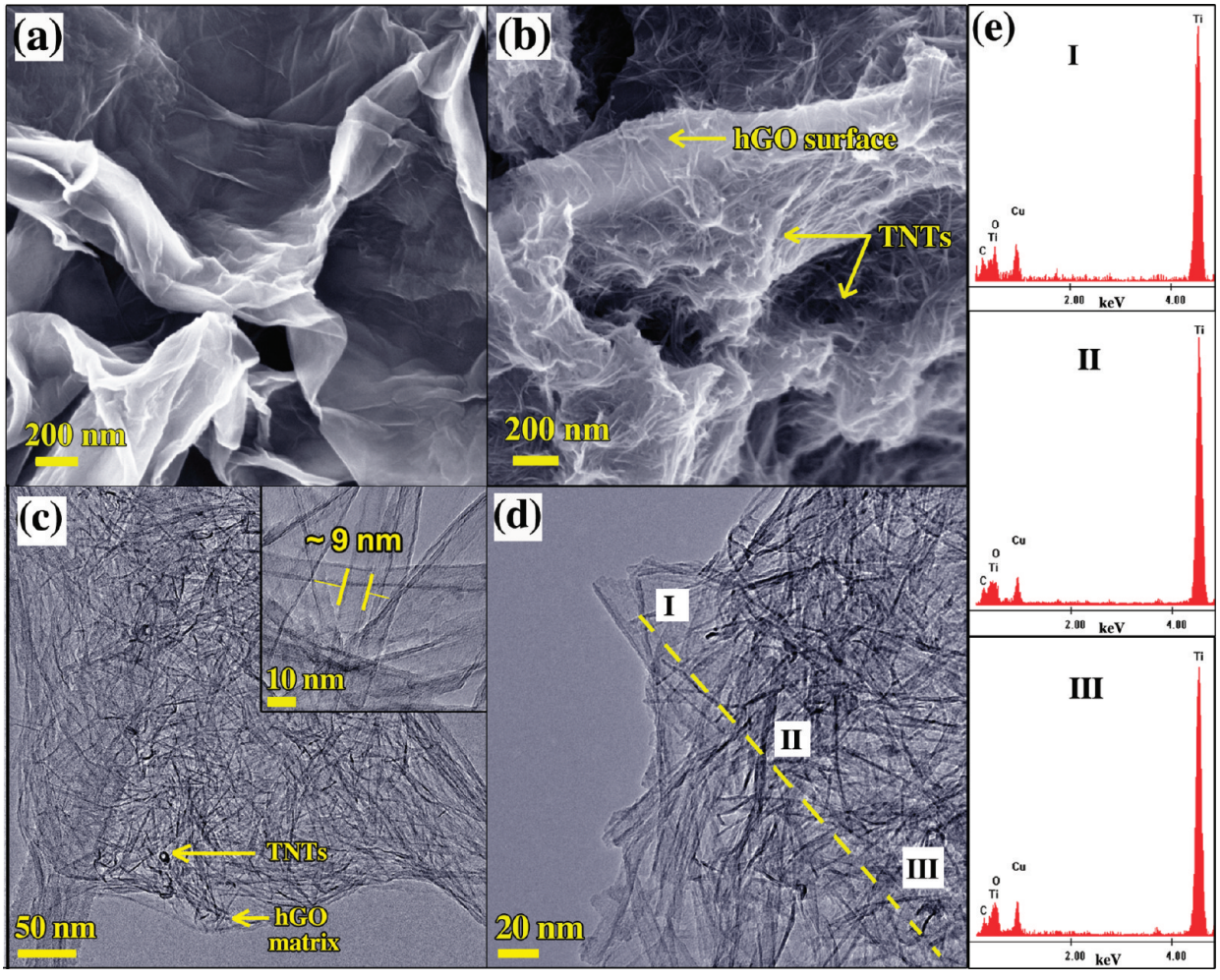

Figure 6. SEM images of (a) GO and (b) 10%-hGO-TNT composites. TEM images of (c) 10%-hGO-TNT composite (inset shows the high resolution TEM image of TNTs on the hGO surface). EDX spectra of three different arbitrary areas (I, II, and III) along a diagonal line of the TEM image of the 10%-hGO-TNT composites (d, e).

dx.doi.org/10.1021/cs200621c | ACS Catal. 2012, 2, 949−956

and the surface of the hGO is covered with an interconnected network of TNTs. (Figure 6b). The TEM image of hGO sheets covered with TNTs is shown in Figure 6c. The as prepared GO exhibits a typical layered morphology. The TEM image shows that the hGO acts as a matrix for the densely packed TNTs. It can be seen that TNTs occupy most of the available surface area of hGO, giving much higher loadings of TNTs in the composite. As seen in the Figure 6c inset, TNTs on the hGO surface have inner and outer diameters of ~6 nm and ~9 nm respectively. These TNTs are slightly smaller than bulk TNTs (~10 nm) prepared under the same conditions.[8] The pore size of the hGO-TNTs (~6 nm) is much larger than the bulk TNTs (3 nm). This implies the precursor titanate sheets are smaller on the hGO and do not scroll as tight. The elemental analysis of the composite was carried out by acquiring EDX spectra of three arbitrary areas (I, II, and III) along a diagonal line of the TEM image (Figure 6d,e). All three EDX spectra of the TEM shows peaks correspond to C and Ti, which ensures that the TNTs are grown on the hGO surfaces (EDX peak corresponds to Cu is from the TEM sample holder grid). The TNT distribution on the hGO surface was further analyzed by EDX mapping (Supporting Information, Figure S4). The EDX spectra obtained from TEM analysis confirms the presence of Ti, while the EDX maps confirm the distribution of TNTs on the surface of hGO sheets.

It is known that the single layers of reduced graphene oxide tend to aggregate back to the graphite structure because of strong van der Waals interactions. Functionalizing graphene sheets with nanoparticles is particularly helpful in overcoming strong interactions between individual graphene layers. Similarly, the formation of TNTs on hGO sheets also keeps the hGO layers separate and readily suspendable in aqueous medium. Even though hGO shows fewer oxygen species on the surface, these oxygen functional groups contribute to the nucleation and growth of TNTs from TiO_2 nanoparticles. The smaller diameter of the TNTs, the transformation of GO to hGO, and the strong interaction between TNTs and hGO surface are expected to enhance the photocatalytic activity of the composites.

Photocatalytic Performance of hGO-TNT Composites. As shown in the graphical illustration in Figure 7a inset, during the photocatalysis, the mechanism involves three steps. This includes adsorption of the pollutant, absorption of light by the photocatalyst, and charge transfer reactions to create radical species to decompose the pollutants. It is well-known that the carbonaceous materials have extraordinary absorption properties, which is used in various environmental applications. Usually most industrial dyes and related pollutants are aromatic in nature and have the ability to create π-π stacking interactions with the graphene aromatic domains. This adsorption process significantly increases the concentration of the organic molecules near the catalytic surface. The enriched environment of the substances closer to the catalytic surface is an important contributing factor for achieving higher photocatalytic degradation rates (Figure 7a inset, step 1).[58]

Upon irradiation of TiO_2 with light, electrons are excited from the VB to the CB generating holes in the VB (Figure 7a inset, step 2). Photoexcited electrons and holes (step 2) can react with H_2O to create radical oxygen species, which can undergo chain reactions to decompose the pollutants into small molecules (Figure 7a inset, step 3). It is known that the fast intrinsic electron–hole pair recombination (10^{-9} s) results in emission and low catalytic activity. This is mainly due to the

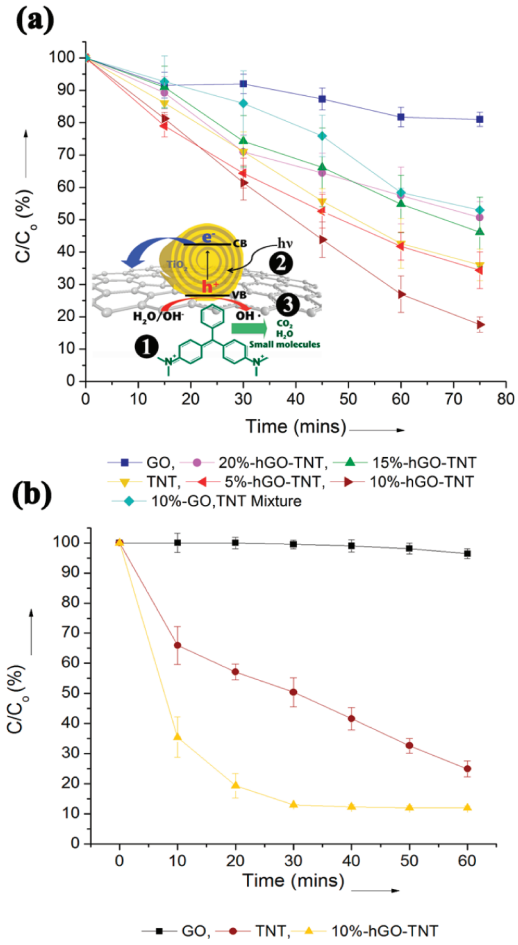

Figure 7. Plot of C/C_o (%) versus time for the photocatalytic degradation of malachite green in (a) a Pyrex reactor and (b) a quartz reactor. Inset image shows a schematic of a proposed model for photocatalytic activity for degradation of malachite green.

adsorption kinetics of pollutants (10^{-8}–10^{-3} s) on TiO_2 being slower than the electron–hole recombination time. Generally, <1% of electrons and holes are trapped and participate in photocatalytic reactions, while the rest recombine without undergoing any chemical reaction.[59] This discrepancy mainly leads to a radiative recombination process and lowers radical concentrations. Therefore, it is important to carefully control step 2 and step 3 to maximize the photocatalytic activity. It has been reported that the CB position of anatase TiO_2 is ~4.2 eV and the work function of graphene is ~4.5 eV with a narrow band gap of 0.26 eV.[13] Therefore, TNTs attached to the graphene sheets inject electrons from TiO_2 CB to the hGO eliminating the radiative electron–hole recombination.[60] It is known that the chemical reduction of GO only partially restores the sp^2 hybridized network.[58] Therefore, remaining oxygen sites are still able to accept electrons and undergo reduction.

The effect of the ratio of hGO to TNT in the composite on the photocatalytic activity was studied in a Pyrex reactor. A control experiment was also performed with TNTs only, which is an excellent photocatalyst under UV radiation. Figure 7a shows a plot of the photocatalytic degradation of malachite green using hGO-TNT samples having 5%, 10%, 15%, and 20% hGO.

dx.doi.org/10.1021/cs200621c | ACS Catal. 2012, 2, 949–956

The amount of the graphene in the composite greatly affects the photocatalytic performance. On the basis of photodegradation rates, 5% and 10% of hGO-TNT show enhanced photocatalytic decomposition compared with just TNTs. In contrast, 15% and 20% hGO-TNT exhibit lower catalytic efficiencies than TNTs. Although higher content of hGO can adsorb large quantities of pollutants, it can limit the contact surface of TNTs with the light leading to lower photocatalytic performance. This effect was clearly observed in the 20%-hGO-TNT composite as it has excess hGO sheets, which partially block the irradiation. Thus, the overall catalytic efficiency is in the order 20% < 15% < 5% < 10% of hGO content. It can be clearly seen that ∼ 80% of malachite green was degraded by 10%-hGO-TNT catalyst over the period of 75 min, concluding that the 10%-hGO-TNT exhibits the highest synergistic effect between TNTs and hGO. A control sample composed of a physical mixture of 10% GO (W/W) and TNT exhibits much lower photocatalytic activity than that of the 10%-hGO-TNT sample. This strongly suggests that the improved photocatalytic activity requires effective charge transfer between TNTs and hGO; thus, close interfacial contact between TNTs and graphene is an essential factor. The 10%-hGO-TNT catalyzed composite led to a higher rate of photodegradation in a quartz reactor than control experiments with TNTs and GO (Figure 7b). The kinetics of the photodegradation of 10%-hGO-TNT, TNTs, and GO was fitted to a pseudo-first order reaction $\ln(C_t/C_o) = -kt$, where k, C_t, and C_o are apparent rate constant, initial concentration, and concentration after a time t of malachite green, respectively. The rate constant calculated for the composite was 0.0674 min^{-1}, which is ∼3 times greater than that of TNTs (0.0218 min^{-1}). The GO does not exhibit notable photocatalytic properties.

Since photocatalytic activity is directly related to the charge recombination rates, photoluminescence spectra of pure TNTs and the composite were analyzed. Photoluminescence arises directly from the charge recombination process of electrons and holes at two different energy states.[61] Supporting Information, Figure S5 shows the PL spectra of the TNTs and the 10%-hGO-TNT composite. PL spectra compares the electron−hole separation, electron−phonon scattering, and electron−hole recombination.[62] The PL spectra of the 10%-hGO-TNT, which has the highest photocatalytic activity and TNTs, which exhibit the lowest catalytic activity, was compared to evaluate the rate of the above processes. The PL spectra show three peaks at 425, 465, and 525 nm that can be attributed to the self-trapped excitons generated on TiO_6 octahedra. Peaks at 465 and 525 nm can be assigned to oxygen vacancy trapped electrons in TiO_2.[62,63] Similar to the CNT/TiO_2 composites, the intensity of the PL spectrum for the 10%-hGO-TNT composite is significantly quenched, suggesting electron transfer from the CB of TiO_2 to the empty electronic states of the hGO. This results in the nonradiative decay of the TiO_2 excited state.[62,64] This observation is consistent with the enhanced charge separation observed for TiO_2 and CNT composites.[65,66] It is noteworthy that the reason for the enhanced photocatalytic activity of 10%-hGO-TNT is the effective charge separation, stabilization, and hindered recombination. Moreover, enhanced photocatalytic activity of the composite also could be a result of the presence of optimum loading of highly conducting hGO and strong coupling between the TNTs and hGO layers.

CONCLUSION

In this study we prepared TNTs on deoxygenated GO/reduced GO sheets, and their photocatalytic activity was evaluated. Various techniques have been developed to prepare TiO_2 nanoparticles-graphene composites, but these studies involved the use of nanoparticles and different reducing agents to convert GO to reduced graphene. The method that we developed has two main advantages for synthesizing novel TiO_2 nanotubes-graphene composites for photocatalysis. First we were able to replace conventional TiO_2 nanoparticle on reduced graphene approach with high surface area TNTs on reduced graphene. Typically, hydrothermally grown TNTs show much higher surface area with outer and inner diameter of ∼9 nm and ∼6 nm. Second, we observed the hydrothermal conditions simultaneously convert GO to a black material that resembles reduced graphene (hGO). As prepared hGO-TNT composite exhibits much higher photocatalytic activity toward the degradation of malachite green than TiO_2 nanotubes itself. The effect of the loading of hGO has been examined by varying different weight ratios of GO starting material. It was found that the much lower and higher additions of hGO lead to lower photocatalytic performance, and the 10% hGO loading exhibits the highest photocatalytic degradation in both UV and a broad visible wavelength range. Thus, we demonstrated that TiO_2 nanotubes can be grown on reduced graphene using TiO_2 nanoparticles and GO via a hydrothermal process. While alkaline hydrothermal treatment converts TiO_2 nanoparticles to TNTs, GO simultaneously deoxygenates to hGO, which has similar graphene content obtained with chemical reducing agents. This novel technique for synthesizing TiO_2 nanotube-graphene based composites could be used to prepare other metal oxide-graphene composites for different applications.

ASSOCIATED CONTENT

Supporting Information

Further details are given in Table S1 and Figures S1−S5. This material is available free of charge via the Internet at http://pubs.acs.org.

AUTHOR INFORMATION

Corresponding Author

*E-mail: balkus@utdallas.edu.

Funding

We thank the National Science Foundation (CBET-0854059) for financial support.

Notes

The authors declare no competing financial interest.

REFERENCES

(1) Chiu, W. H.; Lee, K. M.; Hsieh, W. F. *J. Power Sources* **2011**, *196*, 3683.
(2) Zhang, Y.; Tang, Z. R.; Fu, X.; Xu, Y. J. *ACS Nano* **2010**, *4*, 7303.
(3) Perera., S. D.; Balkus, K. J., Jr. *Mater. Res. Soc. Symp. Proc.* **2010**, *1211*, 115.
(4) Wang, G.; Wang, H.; Ling, Y.; Tang, Y.; Yang, X.; Fitzmorris, R.; Wang, C.; Zhang, J.; Li, Y. *Nano Lett.* **2011**, *11*, 3026.
(5) Wang, D.; Choi, D.; Li, J.; Yang, Z.; Nie, Z.; Kou, R.; Hu, D.; Wang, C.; Saraf, L.; Zhang, J.; Aksay, I.; Liu, J. *ACS Nano* **2009**, *3*, 907.
(6) Ratanatawanate, C.; Chyao, A.; Balkus, K. J. *J. Am. Chem. Soc.* **2011**, 133.
(7) Jin, Q.; Fujishima, M.; Tada, H. *J. Phys. Chem. C* **2011**, *115*, 6478−6483.

(8) Ratanatawanate, C.; Xiong, C.; Balkus, K. J. *ACS Nano* **2008**, *2*, 1682.
(9) Lee, H.; Leventis, H. C.; Moon, S.-J.; Chen, P.; Ito, S.; Haque, S. A.; Torres, T.; Nüesch, F.; Geiger, T.; Zakeeruddin, S. M.; Grätze, M.; Nazeeruddin, M. K. *Adv. Funct. Mater.* **2009**, *19*, 2735.
(10) Asahi, R.; Morikawa, T.; Ohwaki, T.; Aoki, K.; Taga, Y. *Science* **2001**, *293*, 269.
(11) Hirakawa, T.; Kamat, P. *J. Am. Chem. Soc.* **2005**, *127*, 3928.
(12) Subramanian, V.; Wolf, E.; Kamat, P. *J. Phys. Chem. B* **2001**, *105*, 11439.
(13) Yao, Y.; Li, G.; Ciston, S.; Lueptow, R.; Gray, K. *Environ. Sci. Technol.* **2008**, *42*, 4952.
(14) Yen, C.-Y.; Lin, Y.-F.; Hung, C.-H.; Tseng, Y.-H.; Ma, C.-C.; Chang, M.-C.; Shao, H. *Nanotechnology* **2008**, *19*, 045604.
(15) Geim, A. *Science* **2009**, *324*, 1530.
(16) Park, S.; Ruoff, R. *Nat. Nanotechnol.* **2009**, *4*, 217.
(17) Wu, J.; Pisula, W.; Müllen, K. *Chem. Rev.* **2007**, *107*, 718.
(18) Stoller, M.; Park, S.; Yanwu, Z.; An, J.; Ruoff, R. *Nano Lett.* **2008**, *8*, 3498.
(19) Ng, Y. H.; Lightcap, I. V.; Goodwin, K.; Matsumura, M.; Kamat, P. V. *J. Phys. Chem. Lett.* **2010**, *1*, 2222.
(20) Zhang, L. L.; Xiong, Z.; Zhao, X. S. *ACS Nano* **2010**, *4*, 7030.
(21) Zhu, Y.; Murali, S.; Cai, W.; Li, X.; Suk, J.; Potts, J.; Ruoff, R. *Adv. Mater.* **2010**, *22*, 3906.
(22) Singh, V.; Joung, D.; Zhai, L.; Das, S.; Khondaker, S. I.; Seal, S. *Prog. Mater. Sci.* **2011**, *56*, 1178.
(23) Li, X.; Cai, W.; Colombo, L.; Ruoff, R. *Nano Lett.* **2009**, *9*, 4268.
(24) López, V.; Sundaram, R.; Gómez-Navarro, C.; Olea, D.; Burghard, M.; Gómez-Herrero, J.; Zamora, F.; Kern, K. *Adv. Mater.* **2009**, *21*, 4683.
(25) Hummers, W. S.; Offeman, R. E. *J. Am. Chem. Soc.* **1958**, *80*, 1339.
(26) Cassagneau, T.; Fendler, J. H. *J. Phys. Chem. B* **1999**, *103*, 1789.
(27) Muszynski, R.; Seger, B.; Kamat, P. V. *J. Phys. Chem. C* **2008**, *112*, 5263.
(28) Park, S.; An, J.; Potts, J.; Velamakanni, A.; Murali, S.; Ruoff, R. *Carbon* **2011**, *49*, 3019.
(29) Shin, H.; Kim, K.; Benayad, A.; Yoon, S.; Park, H.; Jung, I.; Jin, M.; Jeong, H.; Kim, J.; Choi, J.; Lee, Y. *Adv. Funct. Mater.* **2009**, *19*, 1987.
(30) Su, C.-Y.; Xu, Y.; Zhang, W.; Zhao, J.; Liu, A.; Tang, X.; Tsai, C.-H.; Huang, Y.; Li, L.-J. *ACS Nano* **2010**, *4*, 5285.
(31) Liang, Y.; Wang, H.; Casalongue, H.; Chen, Z.; Dai, H. *Nano Res.* **2010**, *3*, 701.
(32) Lin, X.; Rong, F.; Ji, X.; Fu, D. *J. Sol-Gel Sci. Technol.* **2011**, *59*, 283.
(33) Williams, G.; Seger, B.; Kamt, P. *ACS Nano* **2008**, *2*, 1487.
(34) Zhang, X.-Y.; Li, H.-P.; Cui, X.-L.; Lin, Y. *J. Mater. Chem.* **2010**, *20*, 2801.
(35) Fan, W.; Lai, Q.; Zhang, Q.; Wang, Y. J. *Phys. Chem. C* **2011**, *115*, 10694.
(36) Zhang, H.; Lv, X.; Li, Y.; Wang, Y.; Li, J. *ACS Nano* **2010**, *4*, 380.
(37) Zhang, X.; Sun, Y.; Cui, X.; Jiang, Z. *Int. J. Hydrogen Energy* **2012**, *37*, 811.
(38) Dubin, S.; Gilje, S.; Wang, K.; Tung, V.; Cha, K.; Hall, A.; Farrar, J.; Varshneya, R.; Yang, Y.; Kaner, R. *ACS Nano* **2010**, *4*, 3845.
(39) Chen, Y.; Zhang, X.; Zhang, D.; Yu, P.; Ma, Y. *Carbon* **2011**, *49*, 573.
(40) Rourke, J.; Pandey, P.; Moore, J.; Bates, M.; Kinloch, I.; Young, R.; Wilson, N. *Angew. Chem., Int. Ed.* **2011**, *50*, 3173.
(41) Fan, X.; Peng, W.; Li, Y.; Li, X.; Wang, S.; Zhang, G.; Zhang, F. *Adv. Mater.* **2008**, *20*, 4490.
(42) Shen, J.; Yan, B.; Shi, M.; Ma, H.; Li, N.; Ye, M. *J. Mater. Chem.* **2011**, *21*, 3415.
(43) Sun, W.; Khan, R.; Kim, T. -J.; Kim, W.-J. *Bull. Korean Chem. Soc.* **2008**, *29*, 1217.
(44) Zhang, W.; He, Y.; Zhang, M.; Yin, Z.; Chen, Q. *J. Phys. D.: Appl. Phys.* **2000**, *33*, 912.
(45) Balaji, S.; Djaoued, Y.; Robichaud, J. *J. Raman Spectrosc.* **2006**, *37*, 1416.
(46) Sahoo, S.; Arora, A. K.; Sridharan, V. *J. Phys. Chem. C* **2009**, *113*, 16927.
(47) Santangelo, S.; Messina, G.; Faggio, G.; Donato, A.; De Luca, L.; Donato, N.; Bonavita, A.; Neri, G. *J. Solid State Chem.* **2010**, *183*, 2451.
(48) Solís, D.; Enrique, V. -S.; López, S. H.; Cortés, A. G.; Franco, M. A. −F.; López, M. A. C. *Technol. Adv. Mater.* **2008**, *9*, 25003.
(49) Rao, R.; Podila, R.; Tsuchikawa, R.; Katoch, J.; Tishler, D.; Rao, A.; Ishigami, M. *ACS Nano* **2011**, *5*, 1594.
(50) Kudin, K.; Ozbas, B.; Schniepp, H.; Prud'homme, R.; Aksay, I.; Car, R. *Nano Lett.* **2008**, *8*, 36.
(51) Yoon, I.; Kim, C.-D.; Min, B.-K.; Kim, Y.-K.; Kim, B.; Jung, W.-S. *Bull. Korean Chem. Soc.* **2009**, *30*, 3045.
(52) Shen, J.; Yan, B.; Shi, M.; Ma, H.; Li, N.; Ye, M. *J. Mater. Chem.* **2011**, *21*, 3415.
(53) Zhou, K.; Zhu, Y.; Yang, X.; Jiang, X.; Li, C. *New J. Chem.* **2011**, *35*, 353.
(54) Luo, D.; Zhang, G.; Liu, J.; Sun, X. *J. Phys. Chem. C* **2011**, *115*, 11327.
(55) Acik, M.; Lee, G.; Mattevi, C.; Chhowalla, M.; Cho, K.; Chabal, Y. *Nat. Mater.* **2010**, *9*, 840.
(56) Wang, Y.; Jincheng, L.; Liu, L.; Darren, D. S. *Nanoscale Res. Lett.* **2011**, *6*, 241.
(57) Zhang, H.; Xu, P.; Du, G.; Chen, Z.; Oh, K.; Pan, D.; Jiao, Z. *Nano Res.* **2011**, *4*, 274.
(58) Kamat, P. *J. Phys, Chem. Lett.* **2011**, *2*, 242.
(59) Novoselov, K. *Nat. Mater.* **2007**, *6*, 720.
(60) Zhang, Y.; Tang, Z.-R.; Fu, X.; Xu, Y.-J. *ACS Nano* **2010**, *4*, 7303.
(61) Wu, N.; Wang, J.; Tafen, D. N.; Wang, H.; Zheng, J.-G.; Lewis, J. P.; Liu, X.; Leonard, S. S.; Manivannan, A. *J. Am. Chem. Soc.* **2010**, *132*, 6679.
(62) Wang, F.; Zhang, K. *Curr. Appl. Phys.* **2012**, *12*, 346.
(63) Lei, Y.; Zhang, L.; Meng, G.; Li, G.; Zhang, X.; Liang, C.; Chen, W.; Wang, S. *Appl. Phys. Lett.* **2001**, *78*, 1125.
(64) Liu, J.; Li, J.; Sedhain, A.; Lin, J.; Jiang, H. *J. Phys. Chem. C* **2008**, *112*, 17127.
(65) Yu, H.; Quan, X.; Chen, S.; Zhao, H. *J. Phys. Chem. C* **2007**, *111*, 12987.
(66) Anna Kubacka, A.; Marcos, F. −A.; Gerardo, C. *Chem. Rev.* **2012**, *112*, 1555.